Journal of Ceramic Processing Research. Vol. 14, No. 6, pp. 694~699 (2013)

J O U R N A L O F
Ceramic Processing Research

Effect of ball milling on properties and consolidation of nanostructured ZrO_2 by high-frequency induction heated sintering

In-Jin Shon* and Seung-Mi Kwak

Division of Advanced Materials Engineering and the Research Center of Advanced Materials Development, Engineering College, Chonbuk National University, Chonbuk 561-756, Korea

ZrO_2 powders were high-energy ball milled for various durations and consolidated using the high-frequency induction heated sintering (HFIHS). The effect of milling on the sintering behavior and crystallite size ZrO_2 powders were evaluated. A nanostructured dense ZrO_2 compact with a relative density of up to 96% was readily obtained within 1 min. The ball milling effectively refined the crystallite structure of ZrO_2 powders and facilitated the subsequent consolidation. The sinter-onset temperature was reduced appreciably by the prior milling for 10 hrs. Accordingly, the relative density of ZrO_2 compact increased as the milling time increases. The microhardness and fracture toughness of sintered ZrO_2 increased as the density increases.

Key words: Nanomaterials, Sintering, Mechanical Properties, ZrO_2.

Introduction

ZrO_2, in its pure form, exhibits three well-defined polymorphs. At room temperature, ZrO_2 has a monoclinic crystal structure. The monoclinic structures changes to a tetragonal form above 1170 °C and to a cubic fluorite structure above 2370 °C. The monoclinic/tetragonal transformation in ZrO_2 is thermodynamically reversible but associated with a large volume change (3 to 5%; contraction on heating and expansion on cooling). The cubic phase exists up to the melting point of 2680 °C. However, the addition of certain aliovalent oxides can stabilize the cubic fluorite structure of ZrO_2 from room temperature to its melting point. ZrO_2 has been used for hip and knee joint replacements because of the excellent combination of biocompatibility, low density and corrosion resistance [1]. But coarse-grained ZrO_2 has low wear and abrasion resistance because of its low hardness.

Nanocrystalline materials have received much attention as advanced engineering materials with improved physical and mechanical properties [2, 3]. As nanomaterials possess high strength, high hardness, excellent ductility and toughness, undoubtedly, more attention has been paid for the application of nanomaterials [4, 5]. In recent days, nanocrystalline powders have been developed by the thermochemical and thermomechanical process named the spray con-version process (SCP), co-precipitation and high energy milling [6-8]. However, the grain size in sintered materials becomes much larger than that in pre-sintered powders due to the rapid grain growth during a conventional sintering process. So, controlling grain growth during sintering is one of the keys to the commercial success of nanostructured materials. Unconventional sintering techniques, including high-pressure densification, magnetic pulse compaction and shock densification, have been proposed to overcome the problem of grain growth [9-11]. However, these methods have failed to provide fast, reproducible techniques that yield large quantities of high density samples with nanostructured grains.

The high-frequency induction heated sintering (HFIHS) method has recently emerged as an effective technique for sintering and consolidating high temperature materials [12, 13]. HFIHS is similar to traditional hot-pressing, but the sample is heated by an induced electric current that flows through the sample and a die. This process increases the heating rate (up to 2000 °K minute^{-1}) to a degree much higher than that of traditional hot-press sintering. In this study, we investigated the sintering of ZrO_2 by the HFIHS method. The goal of this research is to produce nanopowder and dense nanostructured ZrO_2 material. In addition, we also studied the effect of high energy ball milling on the sintering behavior, crystallite size and mechanical properties of ZrO_2.

Experimental Procedures

The zirconium oxide powder used in this research was supplied by Alfa, Inc. The powder had a grain size of −325 mesh and was reported to be 99.7% pure. The powder was first milled in a high-energy ball mill (Pulverisette-5 planetary mill) at 250 rpm for various

*Corresponding author:
Tel : +82 63 270 2381
Fax: +82 63 270 2386
E-mail: ijshon@chonbuk.ac.kr

time periods (0, 1, 4, and 10 hrs). Tungsten carbide balls (9 mm in diameter) were used in a sealed cylindrical stainless steel vial under an argon atmosphere. The weight ratio of balls-to-powder was 30 : 1. Milling resulted in a significant reduction in the particle size. The crystallite size of ZrO_2 powders was calculated from the full width at half-maximum (FWHM) of the diffraction peak by Suryanarayana and Grant Norton's formula [14]:

$$B_r(B_{crystalline} + B_{strain}) \cos\theta = k\,\lambda / L + \eta\sin\theta \qquad (1)$$

where B_r is the full width at half-maximum (FWHM) of the diffraction peak after instrumental correction; $B_{crystalline}$ and B_{strain} are FWHM caused by small grain size and internal stress, respectively; k is a constant (with a value of 0.9); λ is wavelength of the X-ray radiation; L and η are the grain size and internal strain, respectively; and θ is the Bragg angle. The parameters B and B_r follow Cauchy's form with the relationship: $B = B_r + B_s$, where B and B_s are the FWHM of the broadened Bragg peaks and the standard sample's Bragg peaks, respectively.

The ZrO_2 powders were placed in a graphite die (outside diameter, 35 mm; inside diameter, 10 mm; height, 40 mm) and then introduced into the induced current activated sintering system (Eltek Co., Korea). A schematic diagram of this method is shown in Fig. 1. The system was first evacuated and a uniaxial pressure of 80 MPa was applied. An induced current was then activated and maintained until the densification rate was negligible, as indicating by the observed shrinkage of the sample. Sample shrinkage is measured in real time by a linear gauge measuring the vertical displacement. Temperatures were measured by a pyrometer focused on the surface of the graphite die. At the end of the process, the induced current was turned off and the sample was allowed to cool to room temperature. The process was carried out under a vacuum of 40 mtorr (5.33 Pa).

The relative density of the sintered sample was measured by the Archimedes method. Microstructural information was obtained from product samples, which had been polished and etched using thermal etching for 1 hr at 950 °C. Compositional and microstructural analyses of the products were made through X-ray diffraction (XRD), field emission scanning electron microscope (FE-SEM) with energy dispersive spectroscopy (EDS). Vickers hardness was measured by performing indentations at a load of 5 kg and a dwell time of 15 s.

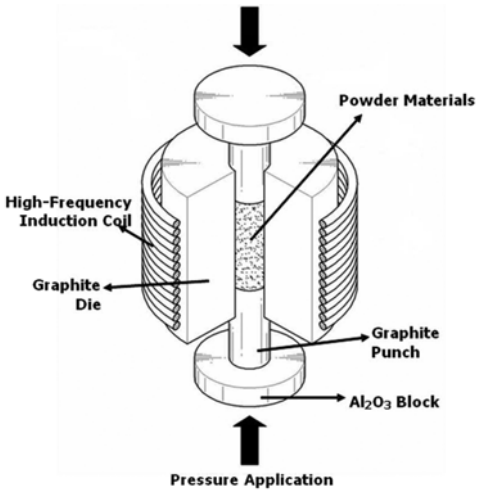

Fig. 1. Schematic diagram of the apparatus for the high-frequency induction heated sintering (HFIHS).

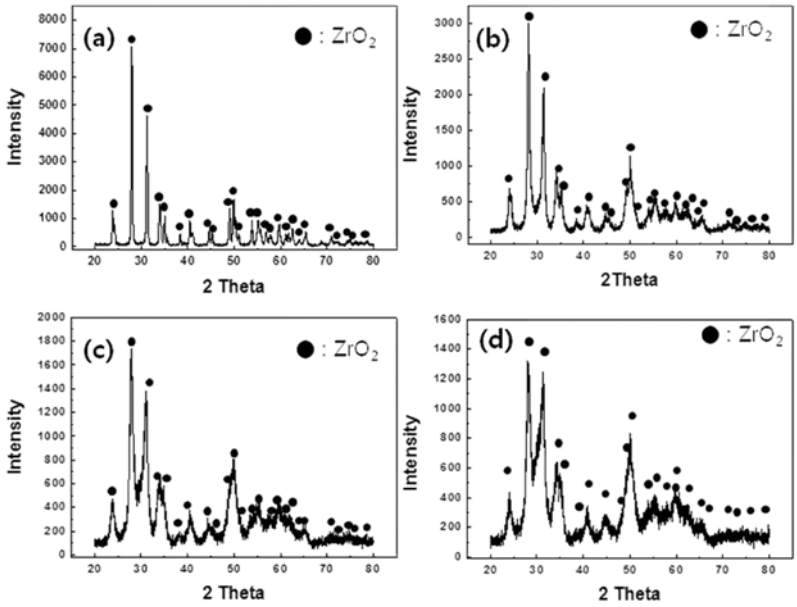

Fig. 2. X-ray diffraction patterns of the ZrO_2 powders after high-energy milling for various durations: (a) as-received (b) milled for 1 hr, (c) milled for 4 hrs and (d) milled for 10 hrs.

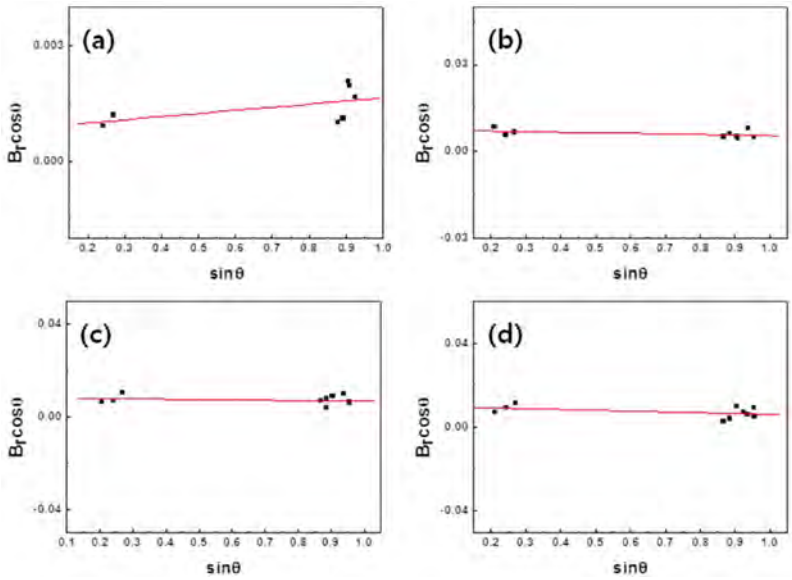

Fig. 3. Plot of Brcosθ versus sinθ for the ZrO2 powders after high-energy milling for various durations: (a) as-received (b) milled for 1 hr, (c) milled for 4 hrs and (d) milled for 10 hrs.

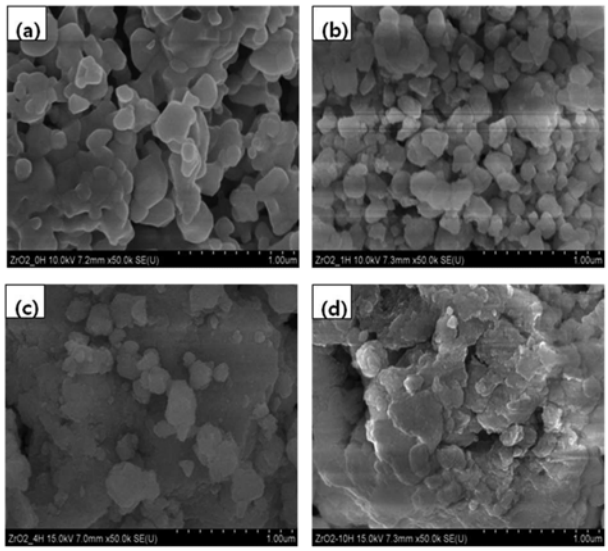

Fig. 4. SEM micrographs of ZrO_2 powders after milling for various durations: (a) as received, (b) 1 hr, (c) 4 hrs and (d) 10 hrs.

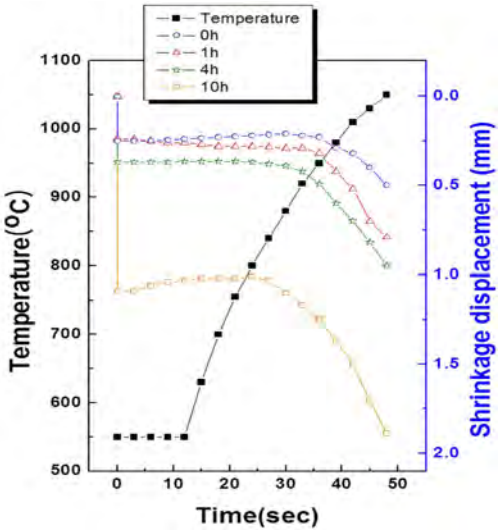

Fig. 5. Shrinkage displacement-temperature curve during the high-frequency induction heated sintering of ZrO_2 powders milled for various durations.

Results and Discussion

Effect of milling on crystallite size

The high-energy milling refined the microstructure of ZrO_2 particles. Fig. 2(a-d) shows X-ray diffraction patterns of the ZrO_2 powders after milling for 1-10 hrs. The broadening of ZrO_2 peaks due to crystallite refinement and strain is evident after milling for 1 hr, and it continuously broadened during the prolonged milling. The milling process is known to introduce impurities from the ball and/or container. However, in this study, peaks other than ZrO_2 were not identified. Plots of Brcosθ versus sinè for the ZrO_2 powders after high-energy milling for various durations are shown in Fig. 3. The ZrO_2 crystallite size by Suryanarayana and Grant Norton's formula was reduced to 19, 17, and 14 nm by milling for 1, 4, 10 hrs, respectively. The crystallite size reduction was most pronounced during the 1st hour of milling. SEM images of Fig. 4(a-d) show the particle size reduction occurred during the high-energy milling process.

Effect of milling on sintering-start temperature

Fig. 5 shows the shrinkage record of ZrO_2 compacts under the applied pressure of 80 MPa. In all cases, there was a brief thermal expansion period as soon as the induced current was applied. After the initial expansion, the shrinkage displacement increases with

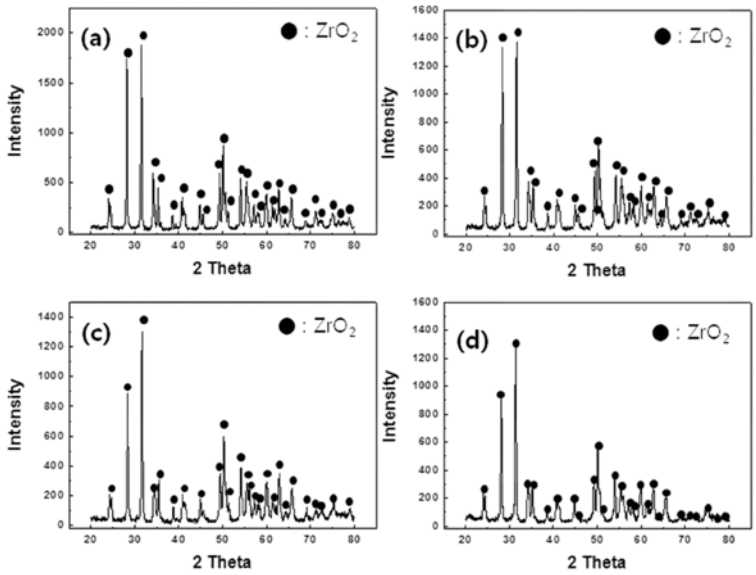

Fig. 6. X-ray diffraction patterns of the sintered compact using ZrO_2 powders after milling for various durations: (a) as-received (b) milled for 1 hr, (c) milled for 4 hrs and (d) milled for 10 hrs.

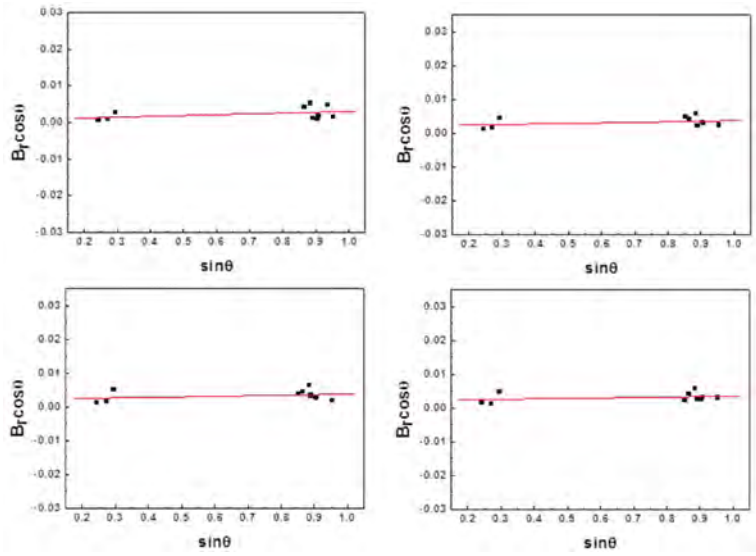

Fig. 7. Plot of Brcosθ versus sinθ for the ZrO_2 sintered after high-energy milling for various durations: (a) as-received (b) milled for 1 hr, (c) milled for 4 hrs and (d) milled for 10 hrs.

heating time and the start of the continuous shrinkage depends on the milling conditions. The amount of shrinkage displacement, which should be indication of densification degree, increases with the milling time. It is clearly seen that the shrinkage-start temperature decreases as the milling time increases. The as-received ZrO_2 powders started to shrink after about 35 s which corresponds to 950 ºC. In contrast, ZrO_2 powders milled for 10 hrs start to shrink at a much lower temperature of 800 ºC. This demonstrates the effectiveness of prior-milling on the densification of ZrO_2 powders. A high-energy ball milling treatment allows the control of the formation of the compound by fixing the reactant powder microstructure. Indeed, high-energy ball milling produces finer crystallites, more strain and defects. Therefore, the consolidation temperature decreases with milling time because the driving force for sintering and contact points of powders for atomic diffusion increases.

Microstructure of ZrO_2 compact

Fig. 6 shows the X-ray diffraction patterns of ZrO_2 sintered from various milled powders. All peaks are ZrO_2 and their peak broadening was seen to reduce suggesting that there would be some grain growth during sintering. Plots of Brcosθ versus sinθ for the ZrO_2 powders sintered after high-energy milling for various durations are shown in Fig. 7. The ZrO_2 crystallite size by Suryanarayana and Grant Norton's formula was reduced to 36, 34, and 32 nm by milling

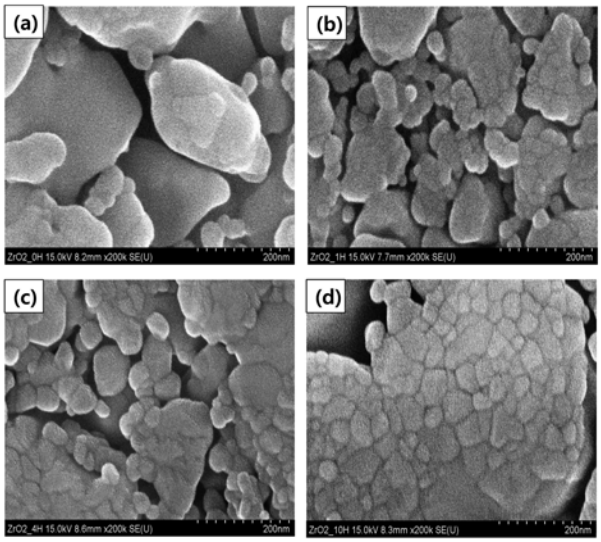

Fig. 8. FE-SEM micrographs showing the polished and etched surface of ZrO_2 compacts: (a) as-received (b) milled for 1 hr, (c) milled for 4 hrs and (d) milled for 10 hrs.

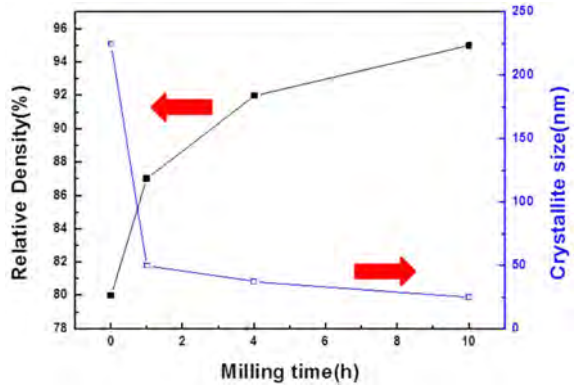

Fig. 9. Variation of relative density and grain size of ZrO_2 sintered from various milled powders.

for 1, 4, 10 hrs, respectively. Fig. 8(a-d) shows SEM images of polished surface of the sintered ZrO_2 compact. The reduction of pore volume with milling time is obvious. It became dense and had more refined microstructure as the milling time increases.

Fig. 9 shows the effect of milling on the crystallite size and relative density for sintered compacts. The crystallite size is seen to decrease significantly by milling and the relative density increases by milling. The crystallite size became larger during sintering suggesting that some grain growth occurred. Nevertheless, the average crystallite size of the sintered ZrO_2 is not greatly larger than that of the milled powders and is still in the nano-scale realm. The retention of the nanoscale crystallite size might be attributed to the high heating rate and the relatively short exposure time of the powders to high temperature in HFIHS. The role of the current (resistive or inductive) in sintering has been the focus of several attempts aimed at providing an explanation of the observed enhancement of sintering and the improved characteristics of the products. The

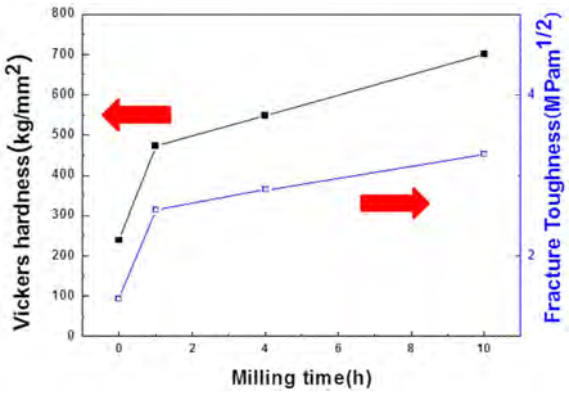

Fig. 10. Variation of hardness and fracture toughness of ZrO_2 sintered from various milled powders.

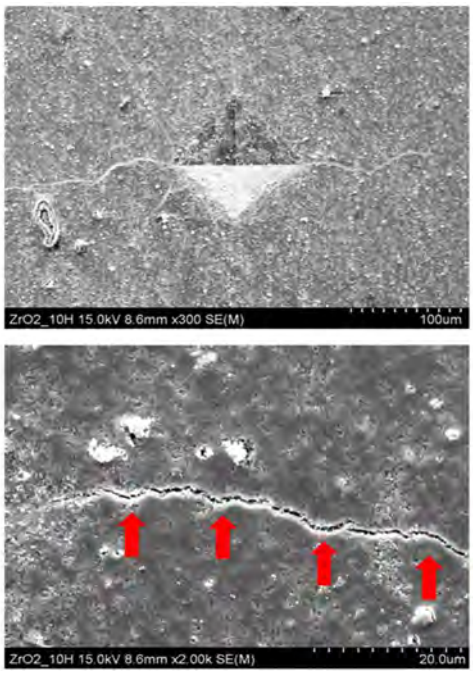

Fig. 11. (a) Vickers hardness indentation and (b) median crack propagating of ZrO_2 sintered from milled powder for 10 hrs.

role played by the current has been variously interpreted, the effect being explained in terms of a fast heating rate due to Joule heating, the presence of a plasma in pores separating powder particles, and the intrinsic contribution of the current to mass transport [15-18].

Mechanical properties of ZrO_2 compact

Vickers hardness and fracture toughness was measured to evaluate the mechanical properties of ZrO_2 compact. Vickers hardness measurements were performed on polished sections of the ZrO_2 samples using a 5 kg_f load and 15 sec dwell time. Indentations with large enough loads produced radial cracks emanating from the corners of the indent. The lengths of these cracks permit estimation of the fracture toughness of the materials by means of the expression [19]:

$$K_{IC} = 0.203(c / a)^{-3/2} \cdot H_v \cdot a^{1/2} \quad (2)$$

where c is the trace length of the crack measured from the center of the indentation, a is one half of the average length of the two indent diagonals, and H_v is the hardness.

Fig. 10 shows the hardness and fracture toughness of ZrO_2 sintered from various milled powders. The hardness and fracture toughness increased as the milling time increased. This effect may be attributed to the refined microstructure and/or higher density. Vickers hardness indentation and a higher magnification view of the indentation median crack in a ZrO_2 sample sintered from milled powder for 10 hrs is shown in Fig. 11, which shows that the crack propagated deflectively (↑).

Summary

ZrO_2 powders were high-energy ball milled for various durations and consolidated using the high-frequency induction heated sintering (HFIHS). The ball milling substantially refined the crystallite structure of ZrO_2 powders and facilitated the subsequent densification process. The consolidation temperature of ZrO_2 powders was reduced by milling because the driving force for sintering and contact points of powders for atomic diffusion increases.

The milling for 10 hrs reduced the crystallite size from 168 nm to 11 nm. The rapid consolidation of the HFIHS process retained the nanostructure after sintering. The microhardness and fracture toughness of ZrO_2 sintered from powders milled for 0, 1, 4, and 10 h were 239, 473, 549, 701 kg/mm^2 and 1.5, 2.6, 2.8, 3.3 MPa · m$^{1/2}$.

Acknowledgments

This research was supported by the Basic Science Research Program through the National Research Foundation of Korea (NRF) funded by the Ministry of Education, Science and Technology (No. 2012001300) and this work was supported by the Human Resources Development program (No. 20134030200330) of the Korea Institute of Energy Technology Evaluation and Planning (KETEP) grant funded by the Korea government Ministry of Trade, Industry and Energy.

References

1. M.N. Rahaman, A. Yao, B.S. Bal, J.P. Garino, M.D. Ries, J. Am. Ceram. Soc. 90 [7] (2007) 1956.
2. M.S. El-Eskandarany, J. Alloys & Compounds. 305 (2000) 225.
3. L. Fu, L.H. Cao, Y.S. Fan, Scripta Materialia. 44 (2001) 1061.
4. N.-R. Park, I.-Y. Ko, J.-K. Yoon, J.-M. Doh, I.-J. Shon, Met. Mater. Int. 17 (2011) 233.
5. S. Berger, R. Porat, R. Rosen. Progress in Materials Science. 42 (1997) 311.
6. Z. Fang, J.W. Eason, Int. J. of Refractory Met. & Hard Mater. 13 (1995) 297.
7. S.L. Du, S.H. Cho, I.Y. Ko, J.M. Doh, J.K. Yoon, S.W. Park, I.J. Shon, Korean J. Met. Mater. 49 (2011) 231.
8. N.R. Park, I.Y. Ko, J.M. Doh, J.K. Yoon, I.J. Shon, Journal of Ceramic Processing Research. 12 (2011) 660.
9. S.C. Liao, W.E. Mayo, K.D. Pae, Acta Mater. 45 (1997) 4027.
10. Z.Q. Jin, C. Rockett, J.P. Liu, K. Hokamoto, N.N. Thadhani, Mater Sci. Forum. 93 (2004) 465-466.
11. V. Ivanov, S. Paranin, V. Khrustov, A. Medvedev, A. Shtolts, Key Eng. Mater. 377 (2002) 206-213.
12. H.S. Kang, I.Y. Ko, J.K. Yoon, J.M. Doh, K.T. Hong, I.J. Shon, Met. Mater. Int. 17 (2011) 57.
13. I.Y. Ko, I.J. Shon, J.M. Doh, J.k. Yoon, S.W. Park, N.R. Park, Journal of Ceramic Processing Research. 12 (2011) 70.
14. C. Suryanarayana, M.G. Norton, X-ray Diffraction: A Practical Approach, Plenum Press, New York (1998).
15. Z. Shen, M. Johnsson, Z. Zhao and M. Nygren, J. Am. Ceram. Soc. 85 (2002) 1921.
16. J.E. Garay, U. Anselmi-Tamburini, Z.A. Munir, S.C. Glade and P. Asoka- Kumar, Appl. Phys. Lett. 85 (2004) 573.
17. J.R. Friedman, J.E. Garay, U. Anselmi-Tamburini and Z.A. Munir, Intermetallics. 12 (2004) 589.
18. J.E. Garay, U. Anselmi-Tamburini and Z.A. Munir, Acta. Mater. 51 (2003) 4487.
19. K. Niihara, R. Morena, and D.P.H. Hasselman, J. Mater. Sci. Lett. 1 (1982) 12.